Investigating the impact of Cp-T values determined by DSC on the PCM-CFD Model

Iten, M. , Liu, S. , Shukla, A. and Silva, P. D.

Original citation:
Iten, M. , Liu, S. , Shukla, A. and Silva, P. D. (2017) Investigating the impact of Cp-T values determined by DSC on the PCM-CFD Model. Applied Thermal Engineering 117 May, 65-75. DOI: 10.1016/j.applthermaleng.2017.02.021

http://dx.doi.org/10.1016/j.applthermaleng.2017.02.021

Elsevier

Accepted Manuscript

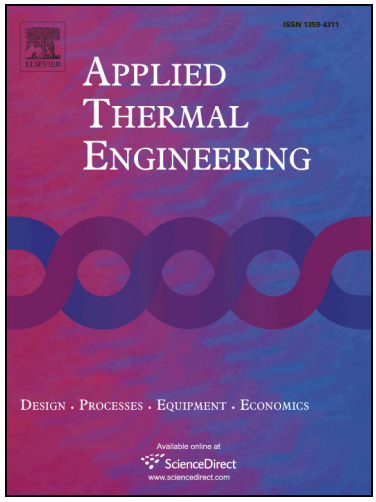

Investigating the impact of C_p-T values determined by DSC on the PCM-CFD Model

M. Iten, S. Liu, Ashish Shukla, P.D. Silva

PII: S1359-4311(16)32500-5
DOI: http://dx.doi.org/10.1016/j.applthermaleng.2017.02.021
Reference: ATE 9902

To appear in: *Applied Thermal Engineering*

Received Date: 17 October 2016
Revised Date: 30 January 2017
Accepted Date: 4 February 2017

Please cite this article as: M. Iten, S. Liu, A. Shukla, P.D. Silva, Investigating the impact of C_p-T values determined by DSC on the PCM-CFD Model, *Applied Thermal Engineering* (2017), doi: http://dx.doi.org/10.1016/j.applthermaleng.2017.02.021

Investigating the impact of C_p-T values determined by DSC on the PCM-CFD Model

M. Iten[a], S. Liu[a*], Ashish Shukla[a], P. D. Silva[b]

[a] School of Energy, Construction and Environment, Coventry University, Coventry, CV1 2HF, United Kingdom

[b]C-MADE, Centre of Materials and Building Technologies, Department of Electromechanical, University of Beira Interior, 6201-001 Covilhã, Portugal

ABSTRACT

For the numerical analysis of Phase Change Material (PCM) enable energy storage based heating/cooling technologies, thermo-physical properties of PCM are very important inputs. It is of vital significance to thermal characterise of PCM to obtain phase change temperature range and the relationship of specific heat capacity with temperature (C_p-T). This is simply done by using differential scanning calorimetry (DSC). Present paper highlights the importance of experimental heating rate in thermal characterisation of PCM. It has been observed that the heating/cooling rate plays an important factor in studying numerically the charging/discharging behaviour of a PCM. Firstly the recommended heating/cooling rate of 10 °C/min stated in ASTM D 4419 is used for the DSC, followed by the rate of 0.2 °C/min observed in the experimental testing. The phase change temperature range and the C_p-T curves have been determined for the both heating/cooling rates. An experimentally validated CFD model has been developed aiming to predict the thermal performance of PCM and the air outlet temperatures. The effective heat capacity method is applied including the C_p-T obtained from the DSC for both rates. Similar heating rate, as per experimental testing, established significant improvements in the validation results when applied in a CFD model.

Keywords: Phase change materials (PCM); Differential scanning calorimetry (DSC); Computational Fluid Dynamics (CFD), melting and solidification of PCM

* Corresponding author. Tel./fax: +44 (0)24 7765 7822/ +44 (0) 2477658296
E-mail address: shuli.liu@coventry.ac.uk (S. Liu).

1. Introduction

Mathematical models are widely used to obtain appropriate solutions for the thermal behavior and optimization for the performance of thermal energy storage (TES) systems. The phase change of Phase Change Materials (PCMs) falls into the category of moving boundary problems [1]. During the phase transformation process a boundary is noticed which separates the material in its liquid and solid phase [2]. This boundary varies according to time, depending on the rate at which the latent heat is absorbed or released through the boundary.

The moving boundary problem is difficult to sort, due to its inherent non-linear nature at the moving interfaces for which displacement rate is controlled by the latent heat passing through the boundary [3]. This problem was firstly noticed when studying the thickness of ice and therefore the problem of freezing is commonly denominated as the "Stefan problem". Significant developments have been presented in the literature for the determination of the "Stefan problem". Overall, solution of the Stefan problem can be determined through analytical and/or numerical formulation. Among the analytical formulations, the most common method is the Neumann method. Whereas for the numerical formulation the enthalpy method and effective heat capacity methods are commonly reported [2]. These methods are further described by Iten and Shuli [2] and the governing equations, for each, are presented.

Most of the available models are numerical, as analytical solutions only exist for simplified geometries and boundary conditions [4]. Numerical modelling of PCMs has been researched for several years and different approaches have been used [3]. Meantime, computational models for the simulation of the melting and solidification processes of PCMs have become available in numerical simulation software. For instance, FLUENT software [5] offers a model denominated as solidification and melting model enabling the study of the phase change of materials through the enthalpy method. In the recent years significant

researches have been carried out using this model and useful agreements have been obtained with the experimental results [6-8]. However there are limitations associated to this model [5] specifically via the lever rule (assuming that the enthalpy-temperature relationship is linear, the melting and solidification of the enthalpy-temperature relationship is therefore similar). In other words, modelling in FLUENT does not provide the flexibility to vary the relationships of enthalpy to temperature and the possibility of introducing temperature hysteresis exists [9]. This limitation presented the discrepancies between the experimental and numerical results [9-11]. To overcome this issue, Chiu and Martin [12] proposed finite-difference conduction based numerical model with enthalpy method. This integration was recognized appropriately since the phase transformation process of the considered PCM (as most of commercial PCMs) occurs over a temperature range rather than a specific temperature point. Numerical and experimental results show the accordance within 5% difference in terms of charge and discharge time in thermal cycling [12]. The same approach of coupling the C_p-T relationship, to characterise the latent heat of PCMs, has been reported in Raj and Velraj [13], Diarce et al. [14], Allouche et al. [15] and Fang et al. [16].

The C_p-T relationship is commonly obtained through Differential Scanning Calorimetry (DSC) testing. However, the correctness of this method depends on the reliability of the procedure adopted for the measurement of the sample. In the DSC testing special attention needs to be given to the selected heating/cooling rates as different heating rates produce different results for the heat flux and phase change temperatures [17, 18]. The authors observed that the melting peak becomes increasingly broad, on a temperature scale, as the heating rate increases. Consequently, also the specific heat values for a certain sample will differ for different heating rates. Standard heating/cooling rates for DSC analysis are reported, such as 10°C/min [19] and 5°C/min [20]. Moreover, Castellón et al. [21] and Günther et al. [22] showed that measurements of PCM using DSC needed a slow heating and

cooling rate, usually lower than 1°C/min, which does not comply with the typical standards used in DSC analysis of polymers or other substances [20]. Furthermore, Raj and Velraj [13] concluded that the scanning rate of the DSC analysis should be carried out based on the cooling rate/heating rate of the selected application, in order to obtain the correct phase change temperature range of the selected PCM [13]. However, a comparison between numerical and experimental results for different DSC results obtained for different rates has not been reported yet.

Hence, this paper intends to provide numerical model based on more accurate input values. This is achieved by comparing the numerical results for C_p-T relationship obtained under different heating/cooling rates. Two heating/cooling rates are selected, one related with the recommended rate stated in ASTM D 4419 [19] and a second one, based on the experimental rate. Further this research paper presents the DSC equipment specification, calibration procedure and the specific process which are key elements to achieve the right C_p-T relationship curves for the CFD model.

2. Experimental setup

The experimental setup consists of an air-PCM heat transfer unit incorporated into an air duct made from wood due to its low thermal conductivity, aiming to reduce the heat losses to the surroundings. The main air duct presents a length (L), width (W) and height (H) of 2.2 m, 0.25 m and 0.218 m respectively. The air-PCM heat transfer unit corresponds to three metallic containers filled with paraffin RT25 surrounded by air channels. RT25 was selected as it is a commercial paraffin with phase change temperature from 23 °C to 25 °C fulfilling the comfort temperatures in buildings. The air-PCM heat transfer unit is coupled to a heating/cooling unit, an exhaust fan as presented in Fig. 1 and to a range of measuring equipment such as K-type thermocouples and anemometer for the measurements of temperature and air velocity respectively. The PCM temperatures have been measured along

the PCM panels and recorded through a data logger for the charging and discharging processes. Mass flow rate of 0.14 kg/s and air inlet temperature of 38 °C (discharging) and 12 °C (charging) have been investigated.

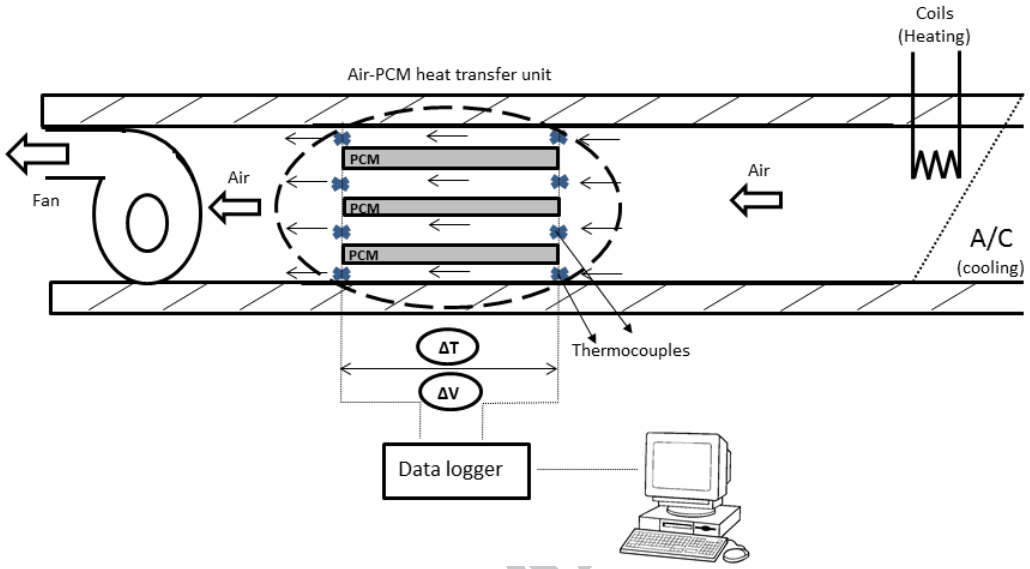

Fig. 1. Experimental Setup

3. Characterising PCM through DSC

Paraffin RT25 has been used in the experimental prototype of the air-PCM unit as shown in Fig.1. A small sample of this paraffin has been analysed through DSC in order to obtain the curve graph of the specific heat capacity and the phase change temperature (C_p-T). A typical DSC response is represented in Fig. 2 for the comparison with the experimental results. It is possible to observe under a certain heating rate, the variation in temperature and heat flux of the analysed sample over a period of time. The C_p-T is then determined as discussed in section 3.5.1 and namely Eq. (1).

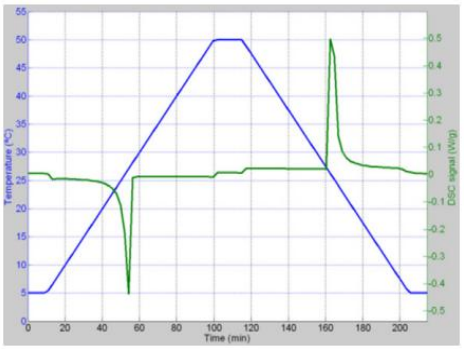

Fig. 2. Typical DSC response (blue line: DSC input heating temperature, green line: sample temperature) [23]

3.1. DSC equipment specification

The DSC equipment used in the present work is the Netzsch brand and the DSC 204 Phoenix model [24]. The equipment includes a calorimetry chamber, a control temperature module, a cooling unit and an acquisition, control system and calculation software. It allows the temperature measured between -170°C and 600°C. The heating of the chamber is accomplished with the thermal resistances integrated in the chamber wall and the temperature is measured by E-type thermocouples. The available heating rate ranges from 0.1 to 99.9 Celsius (°C)/min.

The temperature control of the calorimetry chamber and the temperature defined by the user is achievable by the control modules (TASC 414/3, Netzsch [24]) with a precision of ±0.5°C and a response time of 0.6 seconds. The cooling of the chamber is performed by the use of an external unit (CC 200, Netzsch [24]). Nitrogen is supplied in the chamber for cooling at a pressure of 0.5 bar and with a volumetric flow varying between 5 ml/min and 70 ml/min. The maximum cooling rate allowed for a cooling until the ambient temperature is 70°C/min and it reduced to 40°C/min for further cooling until -140°C. The DSC consists of standard samples, aluminium crucibles and a cold press to seal the crucibles.

3.2. DSC calibration

Due to the complexity associated with the heat transfer mechanisms occurring within the calorimeter chamber, the evaluation of the thermal behaviour of a certain sample is achieved through the previous calibration of the calorimeter. The conditions in which this calibration is carried out should be similar with the samples for analysis. Normally, the process of calibration is based upon the substance with known thermal behaviour (standard sample). Hence, the standard sample calorimetry properties have to be known with precision, namely the phase change temperature, the heat involved in the phase change and the specific heat capacity. The temperature and sensitivity calibration need to be carried out in order to use the calorimeter.

The temperature has to be calibrated due to the temperature sensor being located in the holder rather than in the sample. In the calibration process, the temperature deviation by the sensor and the sample is quantified in order to build a correction curve. The calibration process includes running different standard samples provided by the manufacturer, under similar test conditions detailed in the experimental procedure in section 3.4. The equipment program provides the calibration curves, which requires minimum readings from five standard samples. Similar to Silva [25], in this study total six standard samples of C_6H_{12}, Hg, KNO_3, In, Sn and Bi have been used.

3.3. Experimental heating/cooling rate

The second selected heating/cooling rate is related to the experimental heat transfer rate for the proposed air-PCM heat transfer unit in Fig.1. The experimental heat transfer rate has been determined by subtracting two consecutive temperature readings for a certain thermocouple within the PCM panel. The experimental heating and cooling rates have been

confirmed and displayed in Fig. 3. The temperatures were measured by the thermocouple located at the bottom panel of the storage unit as further detailed in section 5.

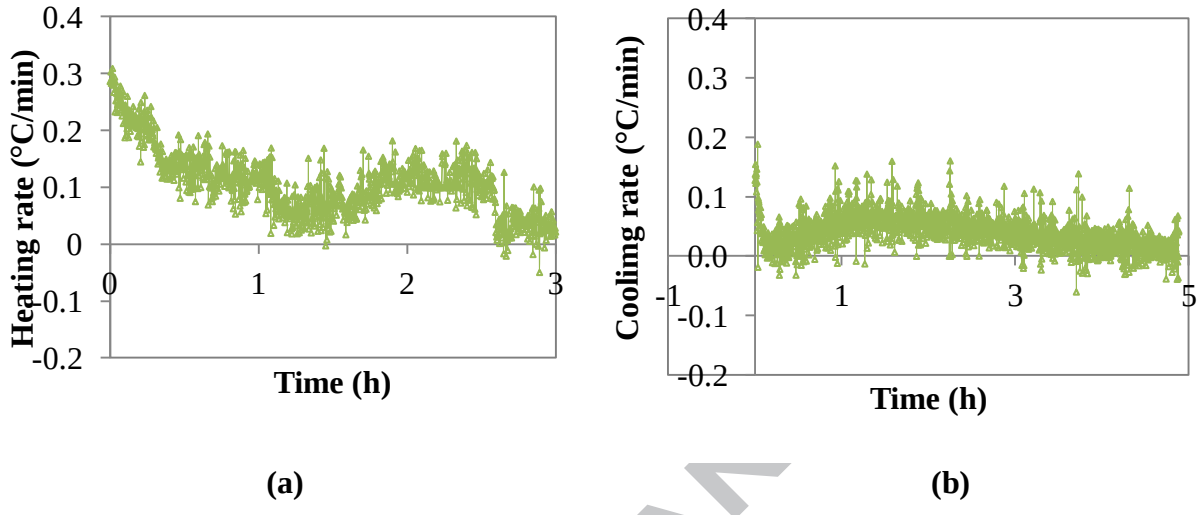

(a) **(b)**

Fig. 3**.** Experimental heating/cooling rates for (a) discharging and (b) charging processes

From Fig. 3 it is observed that the experimental testing for the selected conditions presents heating and cooling rates varying from 0.3°C/min and 0.01°C/min for the discharging (i.e. melting) and charging (i.e. solidification) processes. Hence, the average heating rate of 0.2°C/min is selected.

3.4. DSC experimental procedure

Desired conditions for the testing are very important for DSC measurement such as the temperature range and heating/cooling rates. The selected temperature ranges have been the same for all samples: for the heating process the initial temperature has been setup at -20 °C and the final temperature was at 40°C. The reverse temperature range has been adopted for the cooling process. A heating/cooling rate of 10°C/min and 0.2°C/min with a purge gas flow rate of 25 ml/min has been used for the DSC calibration to test the paraffin sample listed in Table 1. Furthermore, two samples have been run consequently: the reference sample (empty sample) and the sample to be analysed. Two heating and cooling cycles were performed for

each testing and the second cycle has been selected due to the better stabilization of the system.

Table 1
Mass of the samples and the crucibles

Sample	m (mg)	m_{cruc} (mg)	m_{total} (mg)
Reference	0	38.6	38.6
RT25	7.1	38.5	45.6

3.5. DSC results

PCM characterisation using DSC has been carried out under two heat transfer rates (i) Heating rate of 10°C/min recommended by ASTM D 4419 [19] and (ii) Experimental heating rate which is 0.2°C/min.

3.5.1. Heating rate recommended by ASTM D 4419 [19]

The heat flow signal (mW/mg) obtained from the DSC testing for a heating rate of 10°C/min is shown in the Fig. 4. The heat flow variation with the temperatures allows the identification of the region where the phase transition has occurred between the solid and liquid paraffins. The onset, T_{on} and endset, T_{end}, temperatures are the temperatures at which the DSC heat flow curve separates from the baseline indicating the phase change occurrence. T_{peak} corresponds to the temperature at which the maximum heat flow has been registered. The calorimeter also includes a calculation program that allows the determination of the temperatures associated with the phase transition region, following the same procedure as ASTM D 4419 [19]. The T_{on}, T_{end} and T_{peak} are slightly different for melting and solidification due to the apparent hysteresis allied to any phase change process. Table 2 presents a summary of the T_{on}, T_{end}, T_{peak}, and C_p for the selected paraffin. Fig. 4 shows that the phase change of RT 25 has been comprehended between 18 °C and 31 °C for the melting process and 15 °C and 26 °C for the solidification process. The peak temperature (T_{peak}) occurs at 27 °C for the melting and at 21 °C for the solidification with the heat flow peak

(DSC_{peak}) corresponding to approximately 3.2 mW/mg for both processes. The specific heat capacity (C_p) determination are described in ASTM E 1269 [26] and presented by Eq. (1).

$$C_p = \frac{m_{sp}}{m}\frac{V^{DSC}-V_{ref}^{DSC}}{V_{sp}^{DSC}-V_{ref}^{DSC}}C_{p,sp} \quad (1)$$

Where, 'm_{sp}' corresponds to the mass of the standard sample, 'm' to the mass of the sample, kg; 'V^{DSC}' to the DSC signal of the sample, mW/mg; 'V_{ref}^{DSC}'to the DSC signal of the reference sample, mW/mg; 'V_{sp}^{DSC}' to the DSC signal of the standard sample, mW/mg and '$C_{p,sp}$' to the specific heat capacity of the standard sample, J/kg °C. Following Eq. (1), Fig. 4 presents the DSC and C_p-T curve for RT25 material.

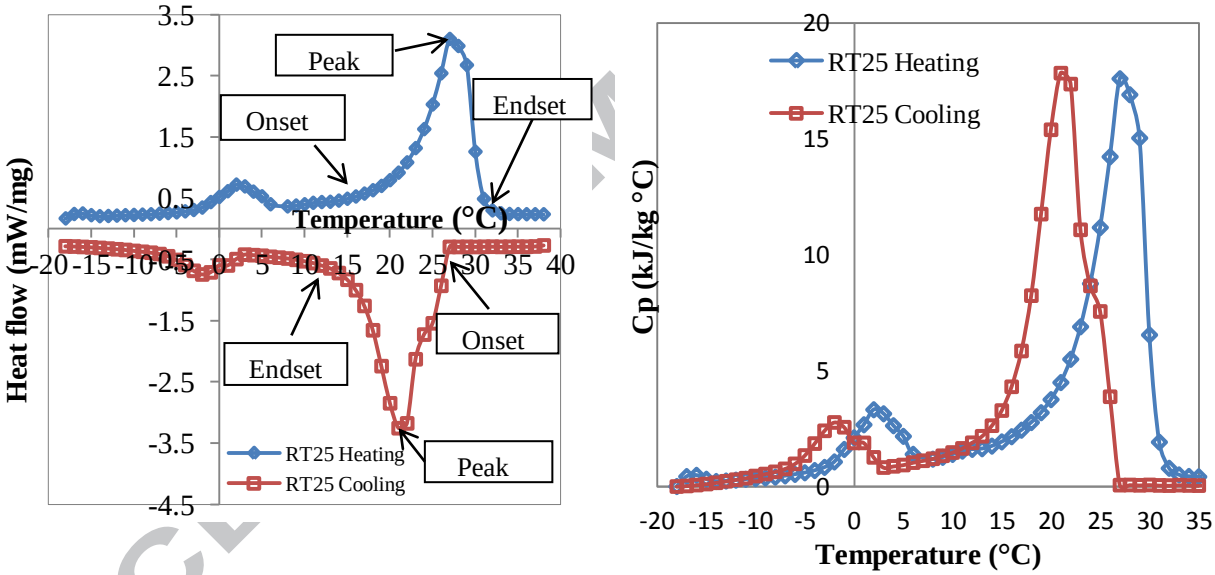

(a) (b)

Fig. 4. a) DSC curve and b) specific heat curve for heating and cooling rate of 10°C/min

Table 2
Summary of the onset (T_{on}), endset (T_{end}), peak temperature (T_{peak}) and peak specific heat capacity ($C_{p,peak}$) for heating and cooling rate of 10°C/min

PCM		T_{on} (°C)	T_{end} (°C)	T_{peak} (°C)	$C_{p,\,peak}$ (kJ/kg °C)
RT25	Heating	18	31	27	17.59
	Cooling	26	15	21	17.83

3.5.2. Experimental heating rate

With the measured heat flow determining the heating/cooling rate of 0.2°C/min applying Eq. (1), it has been possible to determine the specific heat capacity. The heat flow and the specific heat capacity of RT 25 DSC measurement for a heating and cooling rate of 0.2°C/min and 10°C/min are displayed in Fig. 5.

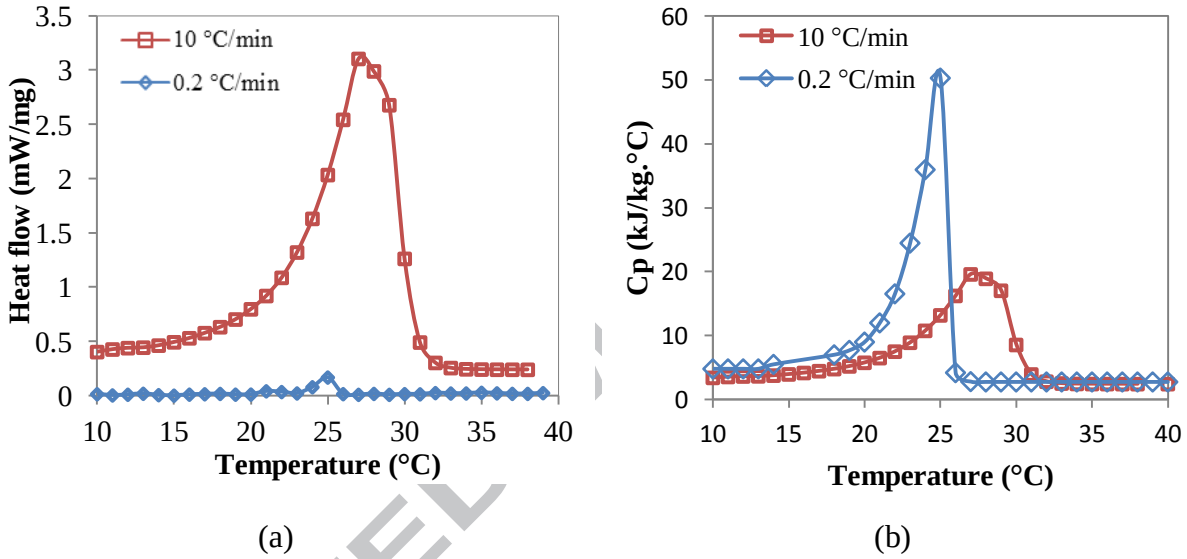

(a) (b)

Fig. 5 a) DSC measurement and b) specific heat (C_p) for 0.2 and 10°C/min heating rates of RT25 paraffin

Overall it has been observed that for a smaller heating rate the phase change range narrows down and the heat flow is reduced, reaching a peak value of 0.2 mW/mg (Fig. 4). On the other hand with a smaller heating rate, higher specific heat capacity values have been achieved (Fig. 5). Table 3 summarizes the phase change temperatures and the specific heat capacity observed for the heating rates of 0.2 and 10 °C/min respectively.

Table 3
Parameters determined from the DSC measurements for the melting process

Heating rate (°C/min)	T_{on} (°C)	T_{end} (°C)	T_{peak} (°C)	$C_{p,peak}$ (kJ/kg.°C)
0.2	22	26	25	50.35
10	18	31	27	17.59

The shapes of the specific heat capacity curves differ considerably for the different heating rates. For lower heating rate, the T_{on} and T_{end} narrow and consequently the T_{peak} shifts towards a lower temperature as indicated in Fig. 5. On the other hand, the $C_{p,peak}$ increases with a smaller heating rate. The same testing has been performed for the cooling of the RT25 samples. The specific heat capacity values for the cooling process have been presented in symmetrical graphs for convenience and in order to differentiate the two processes (see Fig. 6).

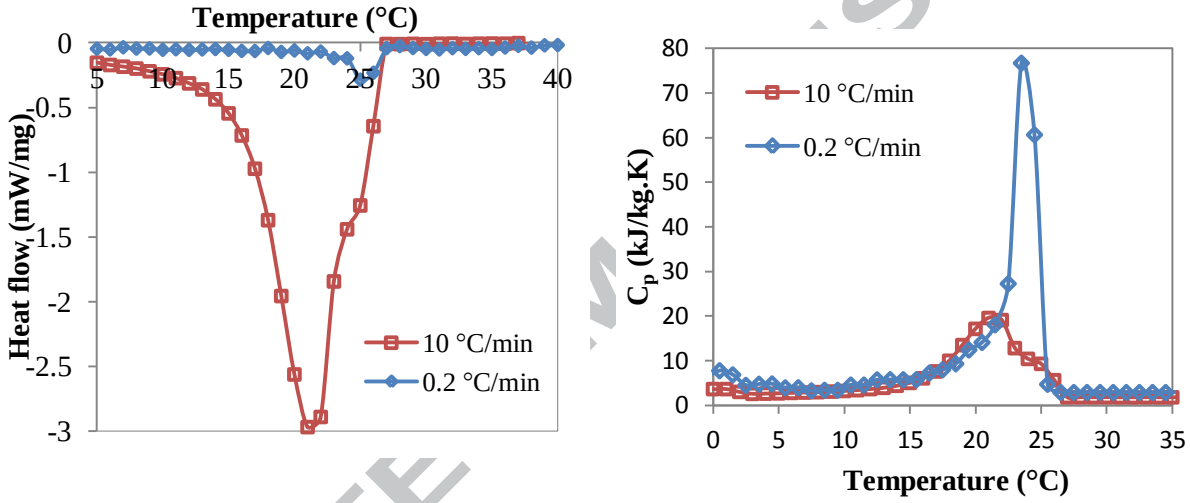

Fig. 6 a) DSC measurement and b) specific heat capacity (C_p) for 0.2 and 10°C/min cooling rates of RT25 paraffin

Similar behaviour has been observed for the cooling process and listed in Table 4. It has been observed that for a lower cooling rate, the phase change temperature range narrows down and the specific heat achieves a much higher value.

Table 4
Parameters determined from the DSC measurements for solidification process

Cooling rate (°C/min)	T_{on} (°C)	T_{end} (°C)	T_{peak} (°C)	$C_{p,peak}$ (kJ/kg.°C)
0.2	26	23	25	60.63
10	26	15	21	17.83

4. C_p-T relationship impact on the CFD modelling

The CFD model intends to predict the temperature inside the PCM and air domains considered in the experimental analysis. The PCM charging and discharging time and the air outlet temperatures will be also simulated. A flow diagram of the CFD procedure is displayed in Fig. 7. The mesh generation considered for the analysis has been described in the section 2 and displayed in Fig. 1. The material properties of the air and steel are introduced according to the CFD database and the PCM properties have been taken from the manufacturer apart from C_p-T relationship, determined by DSC. The boundary conditions have been designed based on the experimental conditions. The mass, momentum and energy equations will be described in section 4.2 and represented in Eq. (2) to Eq. (7). The RNG k-ε has been selected as the turbulence model. Residuals of 10^{-4} for the continuity, velocity and turbulence and 10^{-8} for the energy have been defined. The initial temperature has been set equal to the value of the entire domain.

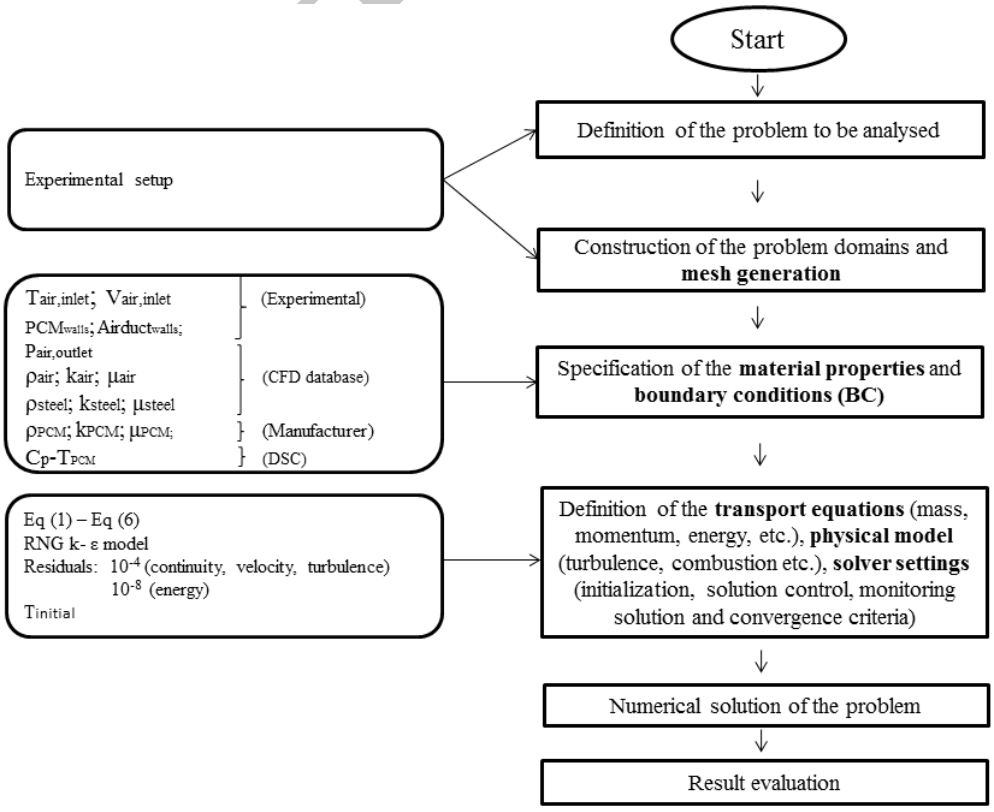

Fig. 7 CFD development and simulation procedure

4.1. Assumptions for the CFD modelling

The investigation of a two-dimensional numerical simulation of the conjugate heat transfer has been conducted using a CFD code FLUENT 15. Two- dimensional model was justified due to the experimental results detailed in Iten et al. [27]. The experiments have shown that the temperature profiles of the PCM was symmetrical along the width of the panel and therefore the simulation can be simplified to a two-dimensional model and reduce significantly the simulation time.

The following assumptions have been made for the CFD analysis.

(i) The air is considered to be incompressible;

(ii) The air flow profile is turbulent;

(iii) The air inlet temperature corresponds to the average inlet temperature within the four air channels;

(iv) The heat transfer in the PCM by convection is negligible compared to the heat transfer due by conduction;

(v) Gravity effect has not been taken into account;

(vi) The density of the PCM in both phases are considered to be constant, independent with temperature but different for solid and liquid state;

(vii) The latent heat value of the PCM has been approximated to the specific heat capacity-temperature relationship and

(viii) The internal thermal resistances and heat across the panel wall are neglected.

The air was considered incompressible as the change of the density was negligible during the flow for the selected conditions. The air flow is assumed turbulent as Reynols number (Re) corresponds to 33883. The heat transfer in the PCM by convection is negligible due to the

minimal height of the panels – 0.02 m and therefore approximated to be a conduction problem.

4.2. Governing equations

The CFD modelling employs the finite volume method for solving the common continuity, momentum and energy equations in particular domains. These equations are known as the Navier-Stokes set of equations and described in Eq. (2), Eq. (3) and Eq. (4) [5].

Momentum equation:

$$\underbrace{\frac{\partial}{\partial t}(\rho\vec{v}) + \nabla(\rho\vec{v})}_{\text{Inertial forces}} = \underbrace{\nabla\left[\mu\left(\nabla\vec{v} + \nabla\overrightarrow{v^{T\prime}}\right)\right]}_{\text{Viscous forces}} \underbrace{- \nabla p}_{\text{Pressure forces}} + \underbrace{\rho\vec{g}}_{\text{External forces applied to the}} \quad (2)$$

Where, t correspond to time, s; T' corresponds to turbulence; ρ corresponds to the density, kg/m^3; μ corresponds to the molecular (dynamic) viscosity, kg/m.s; $\vec{v}$ corresponds to the vector of velocity, m/s and p to the static pressure, Pa.

Continuity equation:

$$\frac{\partial\rho}{\partial t} + \nabla(\rho\vec{v}) = 0 \quad (3)$$

Eq. (3) states that the net accumulation of the mass must be equal to zero, i.e. mass is conserved and incompressible. Eq. (2) and Eq. (3) characterize the fluid flow but no heat transfer hence an additional equation is required. Eq. (4) describes the conservation of energy, describing the heat transferred and then the temperature distribution.

Energy equation:

$$\underbrace{\frac{\partial}{\partial t}(\rho E)}_{\text{Energy stored}} + \underbrace{\nabla[\vec{v}(\rho E + p)]}_{\text{Energy leaving}} = \underbrace{\nabla\left[k\nabla T - \sum_j h_j + \vec{J}_j + (\bar{\bar{\tau}}\vec{v})\right]}_{\text{Energy transfer}} + \underbrace{S}_{\text{Energy generation}} \quad (4)$$

Where, E corresponds to energy, J; k to the thermal conductivity, W/(m. °C); T to temperature, °C; h_j corresponds to the enthalpy, J/kg; $\vec{J_j}$ corresponds to the diffusion flux of species j, mol/(m^2.s); $\bar{\bar{\tau}}$ corresponds to the shear stress, Pa and S corresponds to the heat source, W. In Eq. (4) the first term represents the rate of change of energy with time. In other words how quickly energy is stored. The second term is related to the net convection of energy leaving the system. The third term on the right-hand side represents the net diffusion of energy (energy transfer) into the system due to conduction, species diffusion and viscous dissipation respectively and the fourth term represents any possible heat source generation [5]. The last term is related to the generation within the system by chemical reaction or any other heat source [5]. Overall these equations are difficult to solve through conventional mathematical methods. They are firstly discretised, then linearised and finally solved with a CFD solver through iterative methods.

The effective heat capacity method was proposed by Poirier and Salcudean [28] in order to solve the phase change problem. This method takes into account the phase change as a sensible process with an increased (effective) heat capacity. For this method, the first term in Eq. (4) is approximated to the specific heat. Taking into account the assumptions described in section 4.1 it is simplified as:

$$\frac{\partial}{\partial t}\left(\rho C_{eff}\right) = k\,\nabla T \quad (5)$$

The effective heat capacity method defines a new parameter known as the effective heat capacity (C_{eff}) as follows [29]:

$$C_{eff} = \int_{T_s}^{T_l} \rho C_p \, dT \tag{6}$$

and,

$$C_p = C_{p,s} \qquad if \;\; T < T_s \tag{7a}$$

$$C_p = (1 - f_l)C_{p,s} + f_l C_{p,l} + \frac{L}{T_{l-T_s}} \qquad if \;\; T_s < T < T_l \tag{7b}$$

$$C_p = C_{p,l} \qquad if \;\; T > T_l \tag{7c}$$

Where, $C_{p,s}$ and $C_{p,l}$ correspond to the specific heat in the solid and liquid state respectively. The liquid fraction is represented by f_l and the liquid and solid temperatures are represented by T_l and $T_{s,}$ respectively.

The effective heat capacity method solves the temperatures by iteration between Eq. (5) and Eq. (6). Both methods are applied in the term of the experimental validation and the transient profiles for the PCM and air outlet temperature.

4.3. Geometry, mesh and materials generation

The experimental setup consists mainly an air-PCM unit including metallic rectangular panels filled with commercial paraffin RT25 surrounded by air channels (Fig. 1). The mesh includes 12160 elements and a refinement in the near-wall zones where more complex fluid structures and heat transfer processes are foreseen to occur. The mesh refinement has been performed by varying the mesh sizes at the same ratio through the adapt region tool available on FLUENT 15.0 [5]. The material properties used in the simulations are based upon the following experimental materials: RT25, steel as encapsulation material and air as the working fluid. All the properties are available in FLUENT database apart for RT25. The density, thermal conductivity and dynamic viscosity of RT 25 have been obtained from the

manufacturer data sheet [30] and the values of C_p related to various temperature (C_p-T) under the charging and discharging process are taken from Fig. 3, 4 and 5. The C_p-T relationship is introduced into FLUENT using the piecewise-linear option.

Table 5
Materials properties

Material	Density (kg/m^3)	Thermal Conductivity (W/m°C)	Specific heat (kJ/kg °C)	Dynamic viscosity (kg m/s)
RT25	Solid: 880 Liquid: 760	0.2	Figs. 5b) and 6b)	- 0.0072
Steel	8030	16.27	0.50248	-
Air	1.225	0.0242	1.00643	0.0000179

4.4. Boundary and initial conditions

Overall, the geometry presents six boundary conditions: inlet, outlet, duct walls, PCM panel walls, air and PCM domains as shown in Fig. 8.

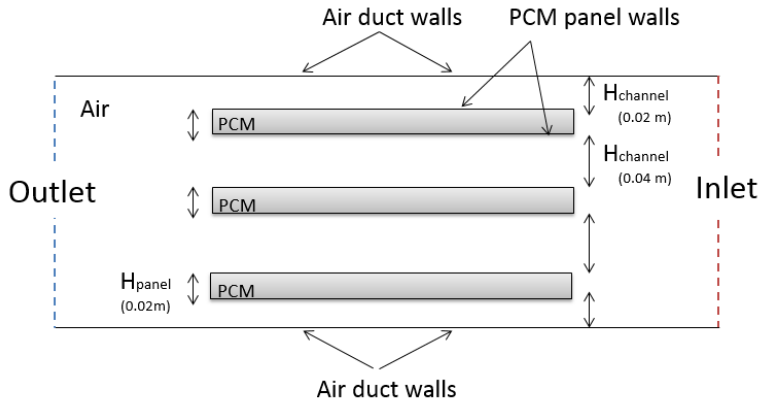

Fig. 8. Boundary conditions of the geometry

The inlet heat transfer fluid has been set as the inlet boundary with a temperature of 38 °C for the discharging process and 12°C for the charging process with a constant mass flow rate of 0.14 kg/s. The outlet cross sectional area of the heat transfer fluid (HTF) has been set as the outlet boundary while the outer surfaces of the PCM panels are set to have a liquid and solid interface with the surfaces of the heat transfer. The air duct surfaces are set as wall

boundaries with a convective boundary related to a constant ambient air temperature of 19 °C and a constant ambient air velocity of zero translating into a constant convective heat transfer coefficient of 10 W/m2 °C. At time t = 0, the stationary PCM is considered to be a solid that keeps at a constant temperature of 16 °C, while the dynamic PCM is set to be a liquid at a constant temperature of 30 °C.

4.5. Operating conditions, turbulence model and solution controls

Firstly the simulations solve the flow and turbulence equations for a steady state until the convergence is reached, followed by an unsteady energy balance equation. The RNG k- ε model has shown to be appropriate to characterise the air profile and will thus be employed in this study. The residual value of 10^{-4} has been set for continuity, velocity and turbulence, and 10^{-8} has been set for energy. Each iteration and convergence has been checked and monitored during the simulations. Beyond these values no significant changes has been observed for the velocity, turbulence and temperature fields. A pressure-based double precision solver has been selected to solve the set of equations with SIMPLE pressure-velocity coupling scheme. The second-order upwind discretization scheme is imposed on the pressure, momentum, density, energy and first-order upwind for the kinetic and dissipation turbulence. The maximum number of iteration for every time step is kept twenty as recommended by Fluent [5].

5. Results and discussion

The specific heat capacity values for RT25 have been obtained through the DSC analysis for two heating rates: 0.2 °C/min and 10 °C/min (section 3.5).

The experimental results presented in Iten et al. [27] that the temperature of the PCM varied significantly along the length of the panels. Therefore, it was crucial to identify the critical

points, i.e. the last part of the PCM reaching the complete melting/solidification. Fig. 9 case 3 presents the theoretical scenario that is observed in the current testing. Fig. 10 displays the temperature contours of the PCM panels over the time, exported from the CFD model. The contours confirm the same critical points presented in Iten et al. [27]: the last part of the PCM reaching the melting temperature in each panel occurred between the centre and left end. Moreover, by comparing these critical points it was observed that the complete melting time of the bottom panel took slightly longer when compared with the top panel and the middle panel. Hence, in this paper, the experimental PCM temperature is also presented with respect to the critical point at the bottom panel.

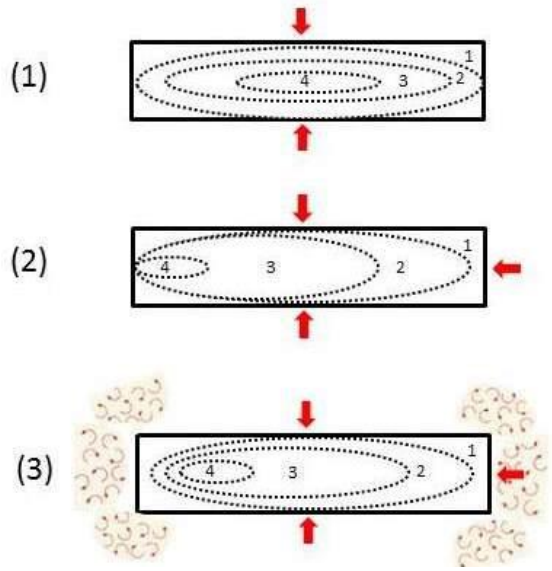

Fig. 9. Melting process of single PCM panel in contact with heat source [27]

The results for the discharging process with an inlet temperature of 38 °C and an air velocity of 2.5 m/s are presented in Fig. 11 for the PCM temperature and in Fig. 12 for the air outlet temperature under the two heating rates.

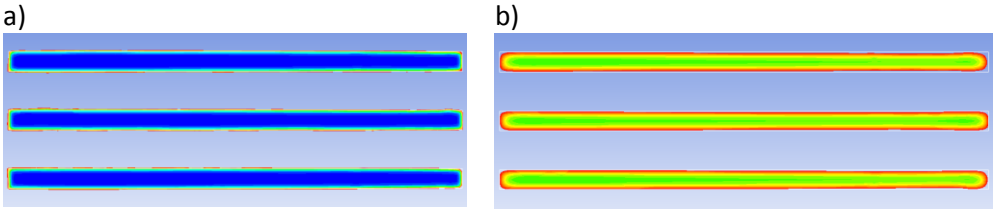

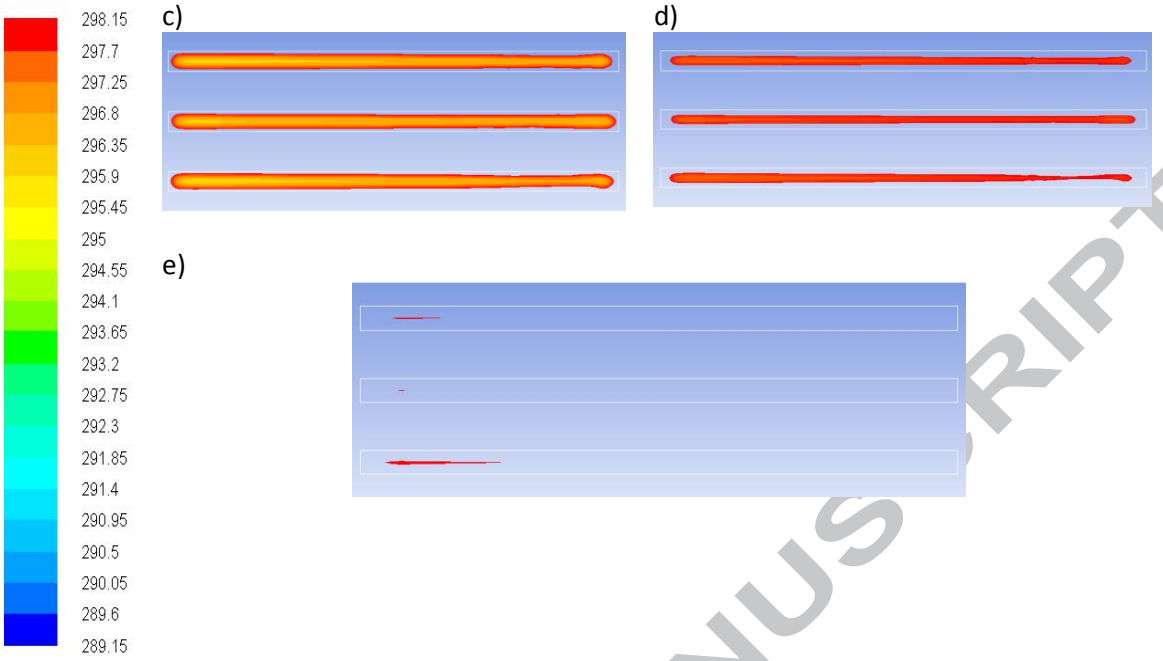

Fig. 9. Temperature contours (discharging process), a) t=0h, b) t=0.5h, c) t=1h, d) t=1.5h and e) t=2h

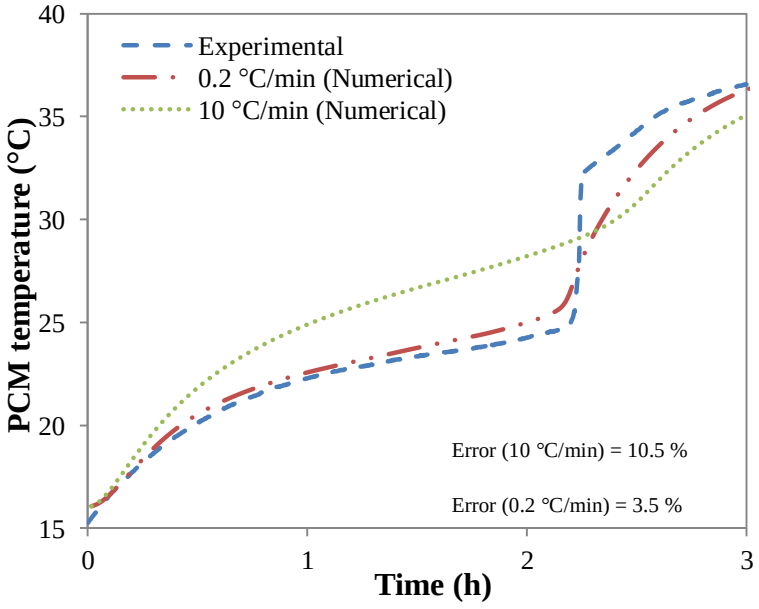

Fig. 10. PCM temperature for the discharging process for DSC heating rates with 0.2 °C/min and 10 °C/min (T= 38 °C, V= 2.5 m/s)

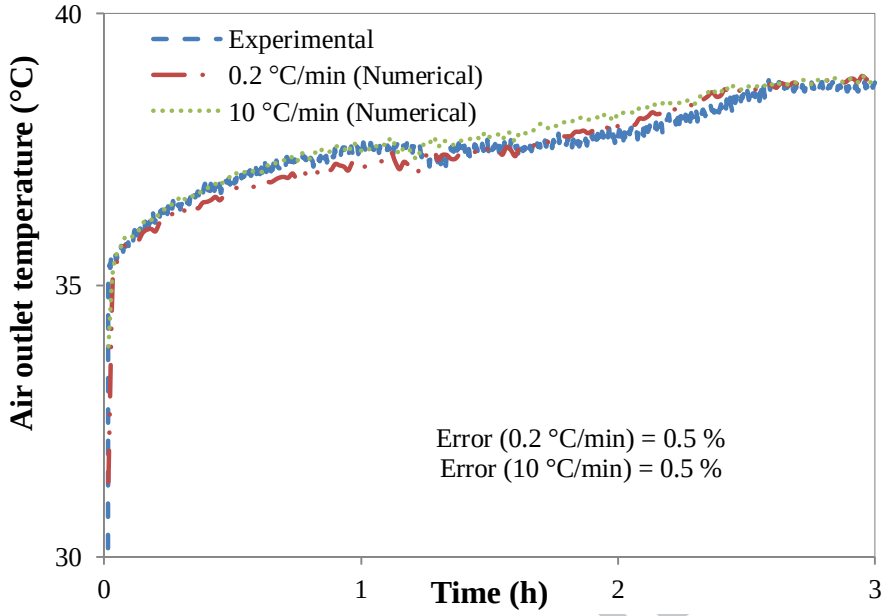

Fig. 11. Air outlet temperature for the discharging process for DSC with heating rates of 0.2 °C/min and 10 °C/min (T= 38 °C, V= 2.5 m/s)

Figs. 11 and 12 show the PCM and air outlet numerical and experimental temperatures. The numerical results for the PCM temperature with a heating rate of 10 °C/min shows a wider phase change temperatures range (18-31°C) deviating 2 to 4 °C from the experimental results. However, the numerical results with heating rate of 0.2 °C/min presents a narrower phase change range (22- 26 °C), closer to the experimental range and shows good agreements over the whole process. The numerical results of the air outlet temperature for both rates have shown good agreements with the experimental results indicating that the air outlet temperature is not very sensitive to the PCM phase change temperature within the CFD model developed based on the specific heat capacity method. Fig. 13 displays the temperature contours of the PCM panels over the time for the charging process. Again, it is observed that the last part reaching the charging temperature of 23 °C (296.15 K) correspond to the critical points. Overall, the charging of the panels was complete after 2.5 h.

Figs. 14 and Fig. 15 present the experimental and numerical results of the charging process of the PCM temperature and the air outlet temperatures for an air inlet temperature of 12 °C and an inlet velocity of 2.5 m/s.

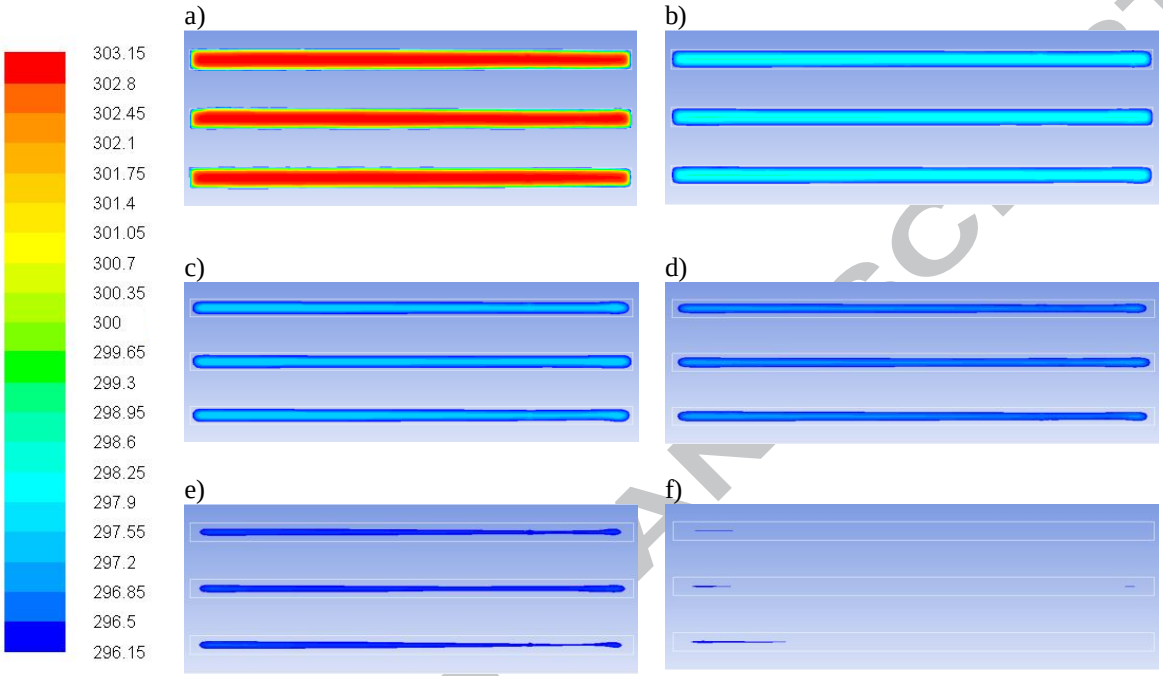

Fig. 12. Temperature contours (discharging process), a) t=0h, b) t=0.5h, c) t=1h, d) t=1.5h, e) t=2h and f) t=2.5h

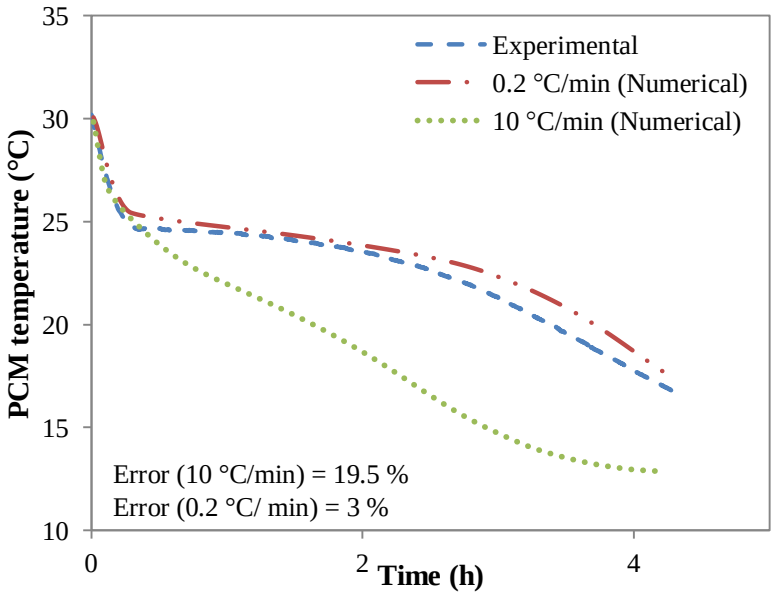

Fig. 13. PCM temperature for the charging process with DSC heating rates of 0.2 °C/min and 10 °C/min (T= 12 °C, V= 2.5 m/s)

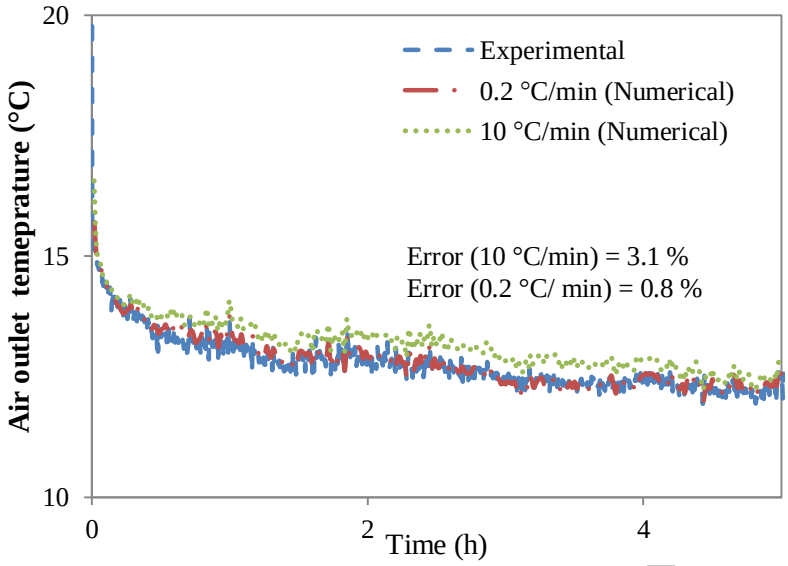

Fig. 14. Air outlet temperature for the charging process with DSC heating rates of 0.2 °C/min and 10 °C/min (T= 12 °C, V= 2.5 m/s)

The numerical results obtained for a cooling rate of 0.2 °C/min shows an improved agreement with the experimental results with an error of only 0.8 % compared to a cooling rate of 10 °C/min presenting an error of 3.1 %. The phase change temperature range for a cooling rate of 10 °C/min corresponds to 26-15 °C, deviating from the experimental phase change range 23-25 °C. The heating rate of 0.2 °C/min however, presented similar range as experimental.

Table 6 displays the errors between the experimental and numerical results, for both processes and both heating/cooling rates, on the PCM temperature and air outlet temperature.

Table 6
Error (%) between experimental and numerical results for PCM temperature and air outlet temperature

Error (%)	0.2 °C /min		10 °C/min	
	Discharging	Charging	Discharging	Charging
PCM temperature	3.5	3	10.5	19.5
Air outlet temperature	0.5	0.8	0.5	3.1

From Table 6, the following conclusions can be drawn: the deviation between the experimental and numerical results are substantially reduced when a C_p-T curve of 0.2 °C/min has been used; the air outlet temperature is not as sensitive as the PCM temperature for the different C_p-T curves; the charging process is significantly affected by the C_p-T relationship, for instance, the error for the PCM temperature is increased by 6 times when C_p-T of 10 °C/min has been applied.

6. Conclusions

It has been proved that the use of a suitable numerical method and the correct thermo-physical properties of the PCM, namely the C_p-T relationship, are the key elements to achieve better agreements between the numerical simulation and the experimental testing results. The validation of the CFD simulation by the experimental results infers that the heating rate of the DSC analysis should be carried out based on the experimental heating/cooling rates. This allows the correct phase change temperature range of the PCM to be obtained. It has been observed that for a heating rate of 10°C/min there was a difference in the temperature range at which the phase change occurred, incurring a deviation between the numerical and experimental results. When the proper C_p-T curves obtained from DSC under the heating/cooling rate of 0.2°C/min, the error between the experimental and numerical results for the PCM temperature has been reduced from 10.5 to 3.5% and from 19.5 to 3.0 % for the discharging and charging process respectively. The air outlet temperature results have been improved significantly for the charging process, the error has been reduced to 0.8 % for the C_p-T curve based on the experimental heating rate.

Moreover, if the experimental phase change temperature range for the given application is used in the thermal characterisation of PCM, the effective heat capacity method based on this range will provide accurate results. To summaries an accurate CFD simulation model for

PCM will be determined by the accuracy of the characteristics of the PCM, which keep varying according to the different heating/cooling environment, but also can be tested and determined through the DSC, if the similar heating/cooling rates have been applied into the DSC testing process. Any CFD model aiming to predict the real life PCM thermal profile will have to consider: the practical application, the proper simulation method and experimentally test the PCM parameters through DSC. The authors intend to extend this study by performing a comparison with the simulation results obtained from PCM manufacturer's data sheet.

References

[1] Zivkovic B, Fujii I. An analysis of isothermal phase change material within rectangular and cylindrical containers. Solar Energy 2001; 70: 51–6.

[2] Iten M, Liu S. A work procedure of utilising PCM as thermal storage systems based on air-TES systems. Energy Conversion and Management 2014; 77: 608-627.

[3] Dutil Y, Rousse DR, Salah NB, Lassue S, Zalewski L. A review on phase-change materials: Mathematical modelling and simulation. Renewable and Sustainable Energy Reviews 2011; 15: 112-130.

[4] Barba A, Spiga M. Discharge mode for encapsulated PCMs in storage tanks. Solar Energy 2003; 74: 141-148.

[5] Fluent. ANSYS FLUENT Release 15.0 User Manual, 2013.

[6] Shatikian V. Melting and Solidification of a Phase-Change Material with internal fins. M.Sc. thesis. Ben-Gurion University of the Negev, Israel, 2004.

[7] Assis E, Katsman L, Ziskind G, Letan R. Numerical and experimental study of melting in a spherical shell. International Journal of Heat and Mass Transfer 2007; 50: 1790- 1804.

[8] Shmueli H, Ziskind G, Letan R. Melting in a vertical cylindrical tube: Numerical investigation and comparison with experiments. International Journal of Heat and Mass Transfer 2010; 53: 4082 – 4091.

[9] Susman G, Dehouche Z, Cheechern T, Craug S. Tests of prototype PCM 'sails' for office cooling. Applied Thermal Engineering 2011; 31: 717-726.

[10] Egolf PW, Manz H. Theory and modelling of phase change materials with and without mushy regions. Journal of Heat and Mass Transfer 1994; 37: 2917-2924.

[11] Kuznik F, Virgone J. Experimental investigation of wallboard containing phase change material: Data for validation of numerical modelling. Energy and Buildings 2009; 41: 561-570.

[12] Chiu JNW, Martin V. Submerged finned heat exchanger latent heat storage design and its experimental verification. Applied Energy 2012; 93: 507-516.

[13] Raj V, Velraj R. Heat transfer and pressure drop studies on a PCM-heat exchanger module for free cooling applications. International Journal of Thermal Sciences 2011; 50: 1573- 1582.

[14] Diarce G, Campos- Celador Á, Martin K, Urresti A, García-Romer A, Sala JM. A comparative study of the CFD modeling of a ventilated active façade including phase change materials. Applied Energy 2014; 126: 307-317

[15] Allouche Y, Varga S, Bouden C, Oliveira AC. Validation of a CFD model for the simulation of heat transfer in a tubes-in-tank PCM storage unit. Renewable Energy 2016; 89: 371-379.

[16] Fang M, Chen G. Effects of different multiple PCMs on the performance of a latent thermal energy storage system. Applied Thermal Engineering 2007; 27:994– 1000.

[17] Mehling H, Cabeza LF. Heat and Cold Storage with PCM: An Up to Date Introduction into Basics and Applications 2008; Page 95, Springer.

[18] Dumas JP, Gibout SG, Cézac P, Franquet E, Haillot D. Model for the DSC thermograms of the melting of ideal binary solutions. Thermochimica Acta 2013; 571: 64-76

[19] ASTM D 4419. Standard test method for measurement of transition temperatures of petroleum waxes by differential scanning calorimetry (DSC), American Society for Testing and Materials; 1990.

[20] ASTM Standard E793. Standard Test Method for Enthalpies of Fusion and Crystallization by Differential Scanning Calorimetry, 2012. American Society for Testing and Materials.

[21] Castellón C, Günther E, Mehling H, Hiebler S, Cabeza LF. Determination of the enthalpy of PCM as a function of temperature using a heat-flux DSC- A study of different measurement procedures and their accuracy. International Journal of Energy Research 2008; 32: 1258-1265.

[22] Günther E, Hiebler S, Mehling H, Redlicj R. Enthalpy of Phase Change Materials as a Function of Temperature: Required Accuracy and Suitable Measurement Methods. International Journal of Thermophysics 2009; 30: 1257-1269.

[23] Barreneche C, Solé A, Miró L, Martorell I, Fernández AI, Cabeza LF. Study on differential scanning calorimetry analysis with two operation modes and organic and inorganic phase change material (PCM). Thermochimica Acta 2013; 553: 23–26.

[24] Netzsch. <https://www.netzsch.com/pt/> [Acessed 20 Apr. 2014].

[25] Silva PD. Modelação matemática e experimental de sistemas de acumulação térmica por calor latente (Dissertation). Universidade da Beira Interior; 2001.

[26] ASTM E 1269. Standard test method for determining specific heat capacity by differential scanning calorimetry, American Society for Testing and Materials; 1995.

[27] Iten M, Liu S, Shukla A. Experimental study on thermal performance of air-PCM unit., Building and Environment 2016; 105: 128-139.

[28] Poirier D, Salcudean M. On numerical methods used in mathematical modelling of phase change in liquid metals, ASME Journal of Heat Transfer 1988; 110: 562–70.

[29] Yang H, He Y. Solving heat transfer problems with phase change via smoothed effective heat capacity and element-free Galerkin methods. International Communications in Heat and Mass Transfer 2010; 37: 385-392.

[30] Rubitherm. <http://www.rubitherm.eu/> [Acessed10 Feb. 2013].

Highlights

- It is of vital significance to thermal characterise Phase Change Materials (PCMs).
- Experimental heating rate is highly important in thermal characterisation of PCMs.
- Similar heating rate, as per experimental testing, established significant improvements in the validation results.